Spatiotemporal complexity of chaos in a phase-conjugate feedback laser system

Tushar Malica, Guillaume Bouchez, Delphine Wolfersberger, Marc Sciamanna

Spatiotemporal complexity of chaos in a phase-conjugate feedback laser system

Tushar MALICA, Guillaume BOUCHEZ, Delphine WOLFERSBERGER and Marc SCIAMANNA

December 12, 2019

An 852 nm semiconductor laser is experimentally subjected to phase-conjugate time-delayed feedback achieved through four-wave mixing in a photorefractive ($BaTiO_3$) crystal. Permutation entropy (PE) is used to uncover distinctive temporal signatures corresponding to the sub-harmonics of the round-trip time and the relaxation oscillations. Complex spatiotemporal outputs with high PE mostly upwards of ∼0.85 and chaos bandwidth (BW) up to ∼31 GHz are observed over feedback strengths up to 7%. Low feedback region counterintuitively exhibits spatiotemporal reorganization and the variation in the chaos BW is restricted within a small range of 1.66 GHz; marking the transition between the dynamics driven by the relaxation oscillations and the external cavity round-trip time. The immunity of the chaos BW and the complexity against such spatiotemporal reorganization shows promise as an excellent candidate for secure communication application.

Keywords : *Semiconductor lasers, Chaos, Phase conjugation, Information theoretical analysis.*

Semiconductor lasers subjected to optical feedback are known to exhibit a diverse range of rich nonlinear effects such as low-frequency fluctuations [1], self-pulsation [2], and chaos [3–8]. Primarily regarding the traditionally undesirable chaotic output, various fields have used it to their advantage and found its application in LIDAR [3, 9], random number generation [4], optical cryptography [5] and secure communication [6]. In the context of optical feedback generated chaos, increased spatiotemporal complexity along with high chaos BW provides a truly secure system for communication. The high BW ensures that these applications display consistent high performance in their respective figure of merits. In addition, the desirability for high spatiotemporal complexity reduces the predictability of the system output. In recent years, several feedback configurations have been proposed for enhancing the chaos BW [4, 10–14]. Particularly in [10], the chaos BW was experimentally shown to improve by many orders of magnitude by substituting a conventional mirror with a phase-conjugate mirror to implement a phase-conjugate feedback (PCF) system. In [15], the complexity of the exhibited chaos in a PCF system was theoretically shown to be significantly of superior quality than observed in a conventional optical feedback system (COF).

In this Letter, we analyze experimentally acquired laser output at varying values of PCF [11, 12]. System outputs are analyzed within the framework of Permutation Entropy (PE). We dissect the underlying system characteristic temporal signatures and correlate it with the observed wide-band chaos. PCF in [11] is achieved by employing a self-pumped total-internal-reflection (CAT) configuration using a photorefractive ($BaTiO_3$) crystal. Presented findings show complex outputs with a complexity > 0.85 for feedback values up to 7%. The complexity is also shown for timescales corresponding to various sub-harmonics of the cavity round-trip time and the relaxation oscillation frequency. A limited range of low feedback values (0.9 % - 2.22 %) with prominent relaxation oscillation frequency, shows deviation from the typical observations of complexity in the parameter space. This is found to correlate with the chaos BW.

Permutation entropy (PE) is applied for quantification of the complexity. This algorithm, developed by Bandt and Pompe [16], is known to measure the predictability of the recurring temporal patterns in a time series through comparison of the relative magnitude of the data points and calculating the probability distribution of user-defined subsets of the time-series. Its extreme robustness to nonlinearity, along with, simplicity and speed of execution make PE an attractive candidate for complexity analysis [16, 17]. Furthermore, it has been employed to a wide range of applications including semiconductor laser

systems [7, 15, 18–20], and the finance sector [21]. The algorithm is detailed in [16, 17] and summarized here. Consider three user-defined parameters, namely, ordinal pattern length (D), length of the time-series (N) and the delay (τ). The ordinal pattern length corresponds to the number of data points extracted from a time-series with each data point τ apart. The delay value is defined as the ratio of the timescale at which one wishes to quantify the complexity to the sampling time (t_{samp}). The widely accepted conditions for the parameters are $3 \leq D \leq 7$ and $N >> D$ [17]. The significantly higher length of the time-series, compared to the ordinal pattern length allows the algorithm to construct many subsets of time-series, known as the ordinal pattern sets (Δ). A maximum of $D!$ number of ordinal patterns may be constructed. The normalized PE (ρ_τ) for a given probability distribution 'p' associated with 'i' integral number of ordinal patterns and timescale 'τ' is mathematically given by:

$$\rho_\tau = \frac{-1}{ln(D!)} \sum_{i=1}^{D!} p(\Delta_i) ln[p(\Delta_i)] \qquad (1)$$

where $0 \leq \rho_\tau \leq 1$ with zero signifying complete predictability while one indicates complete stochasticity. In other words, we visualise a given time series in the form of digitised data points acquired at the sampling time, t_{samp}, storing the amplitude of laser outputs in the complex spatiotemporal domain. The time series follows a helix, wrapped around the helix axis with a constant pitch ($\beta = \tau_x$) with τ_x as the delay at which one wishes to observe the temporal order. The radius of the helix and the number of turns change with the timescale of interest ($= \tau_x.t_{samp}$) for constant length of the helix. An observation axis with length equivalent to the user-defined ordinal pattern length (D) is parallel to the helix axis indicating the data points creating new ordinal patterns. In the presented study, values associated with the timescale corresponding to the external cavity round-trip time ($T_{RT} \simeq$ 10.3 ns) referred to as the round-trip delay ($\tau_{RT} = 824$) and its sub-harmonics will be a major timescale of interest. This is because the laser dynamics are known to evolve at timescales proportional to T_{RT} [7, 8, 15, 20]. To ensure a high resolution analysis, we choose $D = 7$, $N = 36404$, $1\tau = t_{samp}$ =12.5 ps to track changes in the temporal order [17].

The experimental setup shown in Fig. 1 is based on our previous work in [11]. A commercial Fabry-Pérot semiconductor laser (JDS Uniphase DL-SDL-5420) is used with an emission wavelength of 852 nm, the threshold current of 14.9 mA and an operating current range between 20 - 130 mA. The experiment was performed at an operating current of 80 mA and the temperature was maintained at 20°C. The collimating lens is an aspheric objective lens (Newport 5722-B-H) with an effective focal length of 4.5 mm. A beam splitting plate (80:20) redirects the laser emission in three different directions. A part of the transmitted laser beam is coupled into a standard monomode fibre that couples laser emission into a 38 GHz BW photodiode (Newport 1474-A). The free-space optical isolator (Thorlabs IO-3-850-HP) prevents the reflections from the coupler. The system output is acquired as digitized time-series using an oscilloscope (Teledyne LeCroy 10-Zi-A 36 GHz) at a sample rate of 80 GS/s. The part of the laser beam transmitted through the beam splitting plate is used for PCF generated using a Rh-doped BaTiO3 photorefractive crystal (5 mm × 5 mm × 5 mm). At the entrance of the crystal, the laser beam is known to fan or deviate from the expected straight direction due to the beam coupling between the forward propagating incident waves and its scattering caused by the inhomogeneities in the crystal. The deviated laser beam experiences total internal reflection on the different facets of the bulk crystal. Such reflected beams interact among themselves resulting in a phase conjugated backwards propagating laser beam due to the phenomenon of four-wave mixing [22]. The remaining laser emission is fed to a power meter for acquiring the feedback value. The external cavity round-trip time (T_{RT}) is ≃10.3 ns with corresponding cavity length equivalent to ≃1.545 m and an external cavity frequency of ≃ 97.09 MHz.

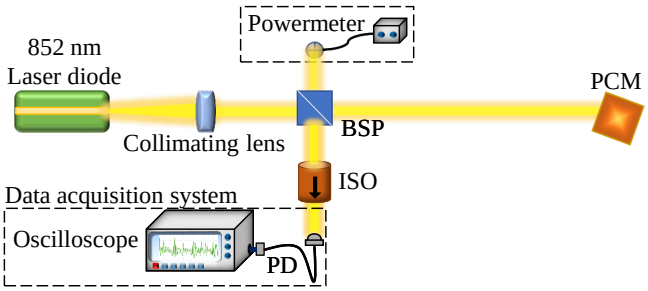

Figure 1: *Laser diode subjected to PCF using a $BaTiO_3$ crystal. BSP: beam splitting plate; PCM: phase-conjugate mirror; ISO: Faraday isolator; PD: photodiode.*

The chaos BW is defined as the upper limit frequency of the RF spectrum containing 80% of the signal energy [11]. It was calculated for every 455.05 ns long time-series for the feedback (η) values between 0 - 7 % as shown in Fig. 2. The exhibited dynamical regimes are divided into four regions. Region I is limited to $\eta < 0.9$ % with high electronic noise resulting in an artificially created high chaos BW. The system transitions from pure noise to the onset of relaxation oscillations followed by the increase in the magnitude of the relaxation oscillation frequency as one approaches region II. The chaos BW is observed to drop by a magnitude of ≃ 10 GHz as the electronic noise becomes a non-contributing factor with increased feedback. Region II is of primary interest in the presented study and encompasses 0.9 % $< \eta <$ 2.22%. It is further described in Fig. 3. The chaos BW is limited to a varied

range of 1.66 GHz before entering region III. This region (2.4 % $< \eta <$ 4.15 %) is dynamically diverse as the strong feedback drives the system into a combination of external cavity modes and pulsing states. Finally in region IV, the external cavity modes are the sole surviving dynamics for $\eta >$ 4.3 %.

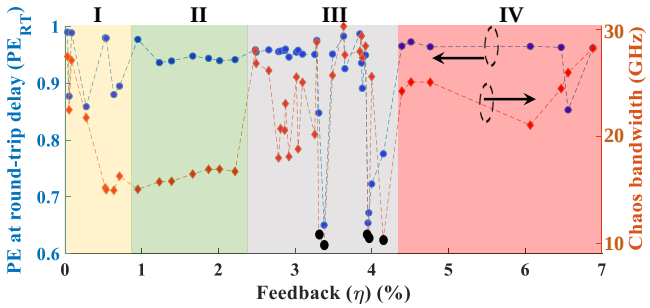

Figure 2: *Dynamics of a PCF system in the context of PE at round-trip delay (primary vertical axis) and chaos BW (secondary vertical axis) as a function of feedback. Region I (yellow): relaxation oscillation buildup; II (green): low-feedback; III (grey): transition window towards external cavity modes (ECM) with black dots representing pulsed output; IV (red): high-feedback with ECM. Black dots represent pulsing states.*

Figure 3 (a) is a 2D representation of the aforementioned helix representation with $\beta = \tau_{RT}$ and the number of turns correspond to the number of round-trips. It is known as a virtual spatiotemporal plot in which the time-delay plays a role analog to a virtual spatial coordinate and the dynamics within one time-delay span is followed as time evolves in units of the time-delay [23]. Such spatio-temporal analogy of the time-delayed laser dynamics has been exploited extensively within the context of the emergence of dissipative spatial solitons [24] or also the study of collective disordered dynamics in otherwise synchronized networks of spatially extended oscillators - also called chimeras [25, 26]. Figure 3(a) is produced by dividing the 455.05 ns long time-series into continuous subsets corresponding to the cavity round-trip time. The horizontal axis represents one round-trip time. Each subsequent subset of the time-series is stacked on top of each other to represent the number of round-trips, i.e., the vertical axis. Each pixel in Fig. 3(a) corresponds to an amplitude of the experimentally acquired data point with the colour scaled in accordance with the colour bar located on the right. Operating conditions in region II exhibit outputs characterized by packets of noise-like signal amplitude spikes when observed over one (or few) cavity round-trips as shown in Fig. 3(b). However, over a few tens of round-trips, some order emerges in the laser dynamics.

Figure 3 (c) shows the typically observed variation in the complexity using PE as a function of delay of the sample time-series shown in Fig. 3 (a) and (b). Recall that a dip in PE value indicates high predictability. A characteristic temporal signature of the laser output is its relaxation oscillation frequency ($f_{RO} \simeq$ 5.2 GHz), twice of which is observed at $\tau = 8 \simeq \tau_{RO}/2$. This is confirmed by the Fourier spectrum analysis of these time series.Time signature corresponding to the relaxation oscillation frequency (τ_{RO}) is observed for the time-series lying in region I. This signature is observed to disappear for the increased values of feedback. Region II is also observed to exhibit temporal signature at a fractional multiple of the f_{RO}, i.e., $(69/2)\tau_{RO}$. The ordinal pattern distribution characteristic to the timescales associated with τ_{RO} are unlike those at τ_{RT}, regardless of the ordinal pattern length. The τ_{RT} of the experimentally acquired time-series is seen at τ_{RT} = 830 as opposed to the previously estimated value of τ_{RT} = 824. This is found to be the case for all the operating conditions observed over regions I - IV. The associated external cavity round-trip time is equivalent to 10.375 ns (96.39 MHz) as opposed to 10.3 ns (97.09 MHz). This slight mismatch between the statistical calculation and experimental observation is due to the inertia of the laser system and includes uncertainty contributed by the oscilloscope's sampling time. Characteristic temporal signatures are also observed for indicated sub-harmonic multiples of the round-trip time seen in Fig. 3 (c).

Figure 2 shows PE value (ρ_{RT}) at τ_{RT} as a function of feedback for the entire parameter space region. The complexity is high, upwards of 0.85, for most operating conditions with an exception to the operating conditions exhibiting stationary dynamics or transitioning to the pulsing states. This is expected as a stable train of pulses will have high predictability. However, outside of region III, i.e., operating conditions lying within 3.3 % $\geq \eta \geq$ 1 % and 4.39 % $\leq \eta \leq$ 6.5 % exhibit $\rho_{RT} >$ 0.93 and are hence, highly complex with extremely low predictability. This is highly advantageous for applications concerning secure communication. Generally speaking, ρ_{RT} as a function of feedback strength is observed to follow the pattern of damped oscillations when observed for $\eta <$ 1% and mostly limits itself between 0.9363 $< \rho_{RT} <$ 0.9869 for $\eta >$ 1%, excluding the exceptions of stable pulsing states having low complexity. Furthermore, Fig. 2 confirms two things. Firstly, the range of ρ_{RT} values in regions I, II and IV measured experimentally agree with the range of values numerically calculated for the theoretical model in [15]. However, the presented system exhibits consistent high complexity (excluding the pulsing states) as a function of feedback strength, contrary to the trend of monotonic increase followed by a plateau and then a slight decrease predicted by the numerics [15]. Secondly, the experimental implementation of COF as in [20] for such long cavity round-trip length (1.35 m for the case in [20]) has $\rho_{RT} \approx$ 0.75 for D = 7 at high injection strength and feedback. Additionally, the complexity of the presented system is also observed to be higher compared to that of a COF system

calculated numerically in [15]. Hence, we experimentally demonstrate that the PCF system is capable of much higher complex outputs restricted to a much lower variation in complexity over a wide range of feedback strength.

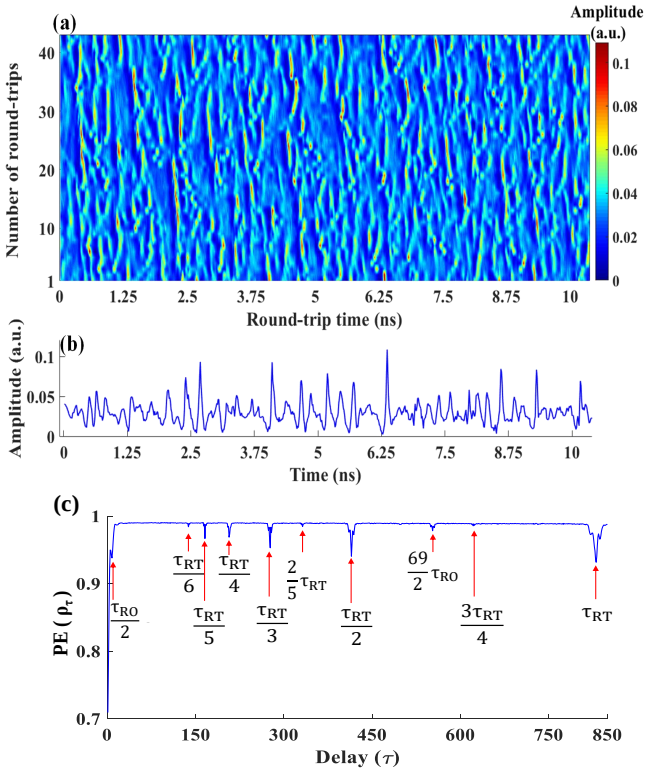

Figure 3: *Typical intracavity dynamics in region II. For $\eta = 1.23$ % (a) Spatiotemporal dynamics observed over multiple round-trips as a function of the round-trip time (ns). The colour bar represents output signal amplitude (a.u.); (b) Sample time-series over one round-trip and, (c) PE (ρ_τ) as a function of delay (τ) showing the general temporal signatures corresponding to the sub-harmonics of cavity round-trip time (τ_{RT}) and the relaxation oscillation frequency (τ_{RO}).*

As a general point, we have established that the PCF system exhibits complex dynamics with high chaos BW. Interestingly, a rearrangement of the complexity between the ordinal patterns is observed uniquely to the region II. This is deduced upon observing the correlation between PE values at the characteristic temporal signatures as seen in Fig. 3 (c) and, the chaos BW as we now discuss. Figure 4 (a) shows the PE values at $\rho_{RT/6}$, $\rho_{RT/5}$, $\rho_{RT/3}$, $\rho_{2RT/5}$, $\rho_{RT/2}$ and, ρ_{RT} as a function of feedback. The PE values lower as one approaches towards τ_{RT} in ascending order of the delay values. Thus, the correlation and the predictability of the ordinal patterns become progressively stronger as the values corresponding to the sub-harmonic multiple of the round-trip time increases. This trend has an exception at $\tau = \tau_{RT/4}$ as indicated using black arrows in Fig. 4 (a). The PE values at $\tau_{RT/4}$ are observed to have a

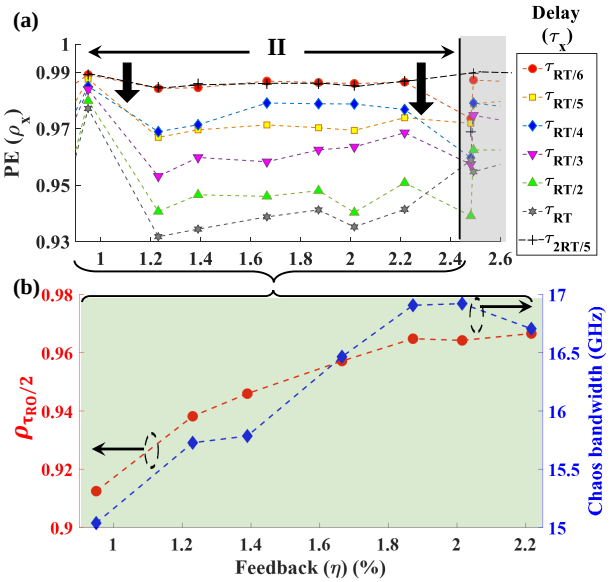

Figure 4: *PE (primary vertical axis) as a function of feedback for (a) τ_x indicated in far-right. Black arrows indicate a change in delay branch position for $\tau = \tau_{RT}/4$. (b) for $\tau = \tau_{RO}/2$. Secondary vertical axis represents the chaos BW. A similar trend observed at $\tau = (69/2)\tau_{RO}$.*

higher value than $\tau_{RT/5}$ and lower than $\tau_{RT/6}$. Outside the window of observation limited to the operating conditions lying in region II, the PE values at $\tau_{RT/4}$ follow the typical general trend of linearly increasing PE values with increasing value of the sub-harmonic round-trip delay. Figure 4 (b) shows the PE value at $\tau_{RO}/2$ steeply increases with an increase in the feedback strength until it saturates before entering region III. Unlike the delay values plotted in Fig. 4 (a), a strong correlation between $\rho_{\tau_{RO}/2}$, $\rho_{(69/2)\tau_{RO}}$ and chaos BW is observed. We emphasise that the subtle complexity reorganization is hidden from isolated analysis of complexity at singular values of delay. Rather, it is revealed upon the comparitive study at specific temporal system signatures and its correlation with chaos BW. The study also highlights (i) such a complexity reorganization of chaos when increasing the feedback rate is obtained while the chaos only shows small variations of its BW and keeps a relatively large BW value; (ii) the chaos BW and the chaos complexity are both associated with peculiar dynamical signatures at T_{RT} and f_{RO}. These features exclusive to region II inform us that the driving dynamics emerge mostly from the undamping of the f_{RO} hence marking a clear transition with the dynamics observe in region III.

Our experimental observations of the presented PCF system shows inherent high spatiotemporal complexity with minimal variation, across a wide range of feedback strengths. From the perspective of complexity, reinforced by the past theoretical analysis, a laser diode subjected to PCF is confirmed to perform better than to COF. Our

findings reaffirm the PCF system as an excellent candidate for applications in secure communication providing consistently high chaos BW with high complexity. The identified system characteristic temporal signatures correspond to the sub-harmonics of the cavity round-trip time and the relaxation oscillation frequency. The study presents distinguishing features exclusive to the region of low (region II) feedback strength, namely, (i) evidence of strong correlation between the relaxation oscillation frequency and the chaos BW, (ii) reorganized spatiotemporal complexity and, (iii) lower values of chaos BW relative to the global range of values. These features demarcate a clean transition between the regions of low and high (region III) feedback strengths. Our study deduces the selective dominance of the regulating dynamics in a PCF system. The system dynamics are governed by the relaxation oscillation frequency at low feedback values, while, the external cavity modes control the system dynamics at high feedback strengths. From a broader perspective, we present here a detailed complexity analysis of a spatiotemporal laser dynamics that emerges from a time-delayed laser system. Such analysis benefits from the computation of PE at different time-scales relative to the laser feedback time-delay and laser internal time-scales. The same technique could apply to obtain deeper insight into temporal order and spatial symmetries of complex unstable, transient and turbulent spatio-temporal dynamics that are commonly encountered, for instance, in the transition to chimera states in networks of coupled nonlinear oscillators.

Région Grand-Est, Moselle, Metz Métropole, European Union (FEDER), Ministry of Higher Education and Research (FNADT), AIRBUS-GDI Simulation.

Disclosures. The authors declare no conflicts of interest.

References

[1] J. Mork, B. Tromborg, and P. Christiansen, "Bistability and low-frequency fluctuations in semiconductor lasers with optical feedback: a theoretical analysis," *IEEE Journal of Quantum Electronics*, vol. 24, no. 2, pp. 123–133, Feb. 1988. [Online]. Available: https://doi.org/10.1109/3.105

[2] C. Mirasso, G. V. Tartwijk, E. Hernandez-Garcia, D. Lenstra, S. Lynch, P. Landais, P. Phelan, J. O'Gorman, M. S. Miguel, and W. Elsasser, "Self-pulsating semiconductor lasers: theory and experiment," *IEEE Journal of Quantum Electronics*, vol. 35, no. 5, pp. 764–770, May 1999. [Online]. Available: https://doi.org/10.1109/3.760324

[3] C.-H. Cheng, C.-Y. Chen, J.-D. Chen, D.-K. Pan, K.-T. Ting, and F.-Y. Lin, "3d pulsed chaos lidar system," *Optics Express*, vol. 26, no. 9, p. 12230, Apr. 2018. [Online]. Available: https://doi.org/10.1364/oe.26.012230

[4] A. Uchida, K. Amano, M. Inoue, K. Hirano, S. Naito, H. Someya, I. Oowada, T. Kurashige, M. Shiki, S. Yoshimori, K. Yoshimura, and P. Davis, "Fast physical random bit generation with chaotic semiconductor lasers," *Nature Photonics*, vol. 2, no. 12, pp. 728–732, Nov. 2008. [Online]. Available: https://doi.org/10.1038/nphoton.2008.227

[5] J.-P. Goedgebuer, L. Larger, and H. Porte, "Optical cryptosystem based on synchronization of hyperchaos generated by a delayed feedback tunable laser diode," *Physical Review Letters*, vol. 80, no. 10, pp. 2249–2252, Mar. 1998. [Online]. Available: https://doi.org/10.1103/physrevlett.80.2249

[6] G. D. VanWiggeren and R. Roy, "Communication with chaotic lasers," *Science*, vol. 279, no. 5354, pp. 1198–1200, Feb. 1998. [Online]. Available: https://doi.org/10.1126/science.279.5354.1198

[7] M. C. Soriano, L. Zunino, O. A. Rosso, I. Fischer, and C. R. Mirasso, "Time scales of a chaotic semiconductor laser with optical feedback under the lens of a permutation information analysis," *IEEE Journal of Quantum Electronics*, vol. 47, no. 2, pp. 252–261, Feb. 2011. [Online]. Available: https://doi.org/10.1109/jqe.2010.2078799

[8] M. Sciamanna and K. A. Shore, "Physics and applications of laser diode chaos," *Nature Photonics*, vol. 9, no. 3, pp. 151–162, Feb. 2015. [Online]. Available: https://doi.org/10.1038/nphoton.2014.326

[9] F.-Y. Lin and J.-M. Liu, "Chaotic lidar," *IEEE Journal of Selected Topics in Quantum Electronics*, vol. 10, no. 5, pp. 991–997, Sep. 2004. [Online]. Available: https://doi.org/10.1109/jstqe.2004.835296

[10] É. Mercier, D. Wolfersberger, and M. Sciamanna, "High-frequency chaotic dynamics enabled by optical phase-conjugation," *Scientific Reports*, vol. 6, no. 1, Jan. 2016. [Online]. Available: https://doi.org/10.1038/srep18988

[11] G. Bouchez, C.-H. Uy, B. Macias, D. Wolfersberger, and M. Sciamanna, "Wideband chaos from a laser diode with phase-conjugate feedback," *Optics Letters*, vol. 44, no. 4, p. 975, Feb. 2019. [Online]. Available: https://doi.org/10.1364/ol.44.000975

[12] É. Mercier, L. Weicker, D. Wolfersberger, D. M. Kane, and M. Sciamanna, "High-order external cavity modes and restabilization of a laser diode subject to a phase-conjugate feedback," *Optics Letters*, vol. 42,

no. 2, p. 306, Jan. 2017. [Online]. Available: https://doi.org/10.1364/ol.42.000306

[13] H. Someya, I. Oowada, H. Okumura, T. Kida, and A. Uchida, "Synchronization of bandwidth-enhanced chaos in semiconductor lasers with optical feedback and injection," *Optics Express*, vol. 17, no. 22, p. 19536, Oct. 2009. [Online]. Available: https://doi.org/10.1364/oe.17.019536

[14] R. Sakuraba, K. Iwakawa, K. Kanno, and A. Uchida, "Tb/s physical random bit generation with bandwidth-enhanced chaos in three-cascaded semiconductor lasers," *Optics Express*, vol. 23, no. 2, p. 1470, Jan. 2015. [Online]. Available: https://doi.org/10.1364/oe.23.001470

[15] D. Rontani, E. Mercier, D. Wolfersberger, and M. Sciamanna, "Enhanced complexity of optical chaos in a laser diode with phase-conjugate feedback," *Optics Letters*, vol. 41, no. 20, p. 4637, Oct. 2016. [Online]. Available: https://doi.org/10.1364/ol.41.004637

[16] C. Bandt and B. Pompe, "Permutation entropy: A natural complexity measure for time series," *Physical Review Letters*, vol. 88, no. 17, Apr. 2002. [Online]. Available: https://doi.org/10.1103/physrevlett.88.174102

[17] M. Riedl, A. Müller, and N. Wessel, "Practical considerations of permutation entropy," *The European Physical Journal Special Topics*, vol. 222, no. 2, pp. 249–262, Jun. 2013. [Online]. Available: https://doi.org/10.1140/epjst/e2013-01862-7

[18] L. Yang, W. Pan, L. Yan, B. Luo, and N. Li, "Mapping the dynamic complexity and synchronization in unidirectionally coupled external-cavity semiconductor lasers using permutation entropy," *Journal of the Optical Society of America B*, vol. 32, no. 7, p. 1463, Jun. 2015. [Online]. Available: https://doi.org/10.1364/josab.32.001463

[19] A. Aragoneses, S. Perrone, T. Sorrentino, M. C. Torrent, and C. Masoller, "Unveiling the complex organization of recurrent patterns in spiking dynamical systems," *Scientific Reports*, vol. 4, no. 1, Apr. 2014. [Online]. Available: https://doi.org/10.1038/srep04696

[20] J. P. Toomey and D. M. Kane, "Mapping the dynamic complexity of a semiconductor laser with optical feedback using permutation entropy," *Optics Express*, vol. 22, no. 2, p. 1713, Jan. 2014. [Online]. Available: https://doi.org/10.1364/oe.22.001713

[21] L. Zunino, M. Zanin, B. M. Tabak, D. G. Pérez, and O. A. Rosso, "Forbidden patterns, permutation entropy and stock market inefficiency," *Physica A: Statistical Mechanics and its Applications*, vol. 388, no. 14, pp. 2854–2864, Jul. 2009. [Online]. Available: https://doi.org/10.1016/j.physa.2009.03.042

[22] J. Feinberg, "Self-pumped, continuous-wave phase conjugator using internal reflection," *Optics Letters*, vol. 7, no. 10, p. 486, Oct. 1982. [Online]. Available: https://doi.org/10.1364/ol.7.000486

[23] F. T. Arecchi, G. Giacomelli, A. Lapucci, and R. Meucci, "Two-dimensional representation of a delayed dynamical system," *Physical Review A*, vol. 45, no. 7, pp. R4225–R4228, Apr. 1992. [Online]. Available: https://doi.org/10.1103/physreva.45.r4225

[24] M. Marconi, J. Javaloyes, S. Barland, S. Balle, and M. Giudici, "Vectorial dissipative solitons in vertical-cavity surface-emitting lasers with delays," *Nature Photonics*, vol. 9, no. 7, pp. 450–455, Jun. 2015. [Online]. Available: https://doi.org/10.1038/nphoton.2015.92

[25] C.-H. Uy, L. Weicker, D. Rontani, and M. Sciamanna, "Optical chimera in light polarization," *APL Photonics*, vol. 4, no. 5, p. 056104, May 2019. [Online]. Available: https://doi.org/10.1063/1.5089714

[26] L. Larger, B. Penkovsky, and Y. Maistrenko, "Laser chimeras as a paradigm for multistable patterns in complex systems," *Nature Communications*, vol. 6, no. 1, Jul. 2015. [Online]. Available: https://doi.org/10.1038/ncomms8752